Ultramicroscopy 136 (2014) 160–164

Contents lists available at ScienceDirect

Ultramicroscopy

journal homepage: www.elsevier.com/locate/ultramic

The post-peak spectra in electron energy loss near edge structure

Feng Tian [a,*], Peter Schattschneider [b], Micheal Stoger-Pollach [c]

[a] School of Materials Science and Engineering, Shanghai University for Science and Technology, 200093 Shanghai, China
[b] Institute for Solid State Physics, Vienna University of Technology, A-1040 WIEN, Austria
[c] Service Center for Electron Microscopy, Vienna University of Technology, A-1040 WIEN, Austria

ARTICLE INFO

Article history:
Received 26 July 2013
Received in revised form
8 October 2013
Accepted 9 October 2013
Available online 17 October 2013

Keywords:
Post-peak spectrum
ELNES
Electron microscopy
Quantitative analysis

ABSTRACT

The origin of post-peak spectra in electron energy lo[ss] near edge structur[e] (ELNES) spectra of pure Ni and NiO is investigated through *ab initio* calculation[s]. Contrary to [the] [co]nventional view that post-peak spectra in ELNES are generated by transitions to continu[um] states, it is fo[und] that orbit hybridization is the main cause of post-peak spectra in the low energy rang[e] above the Fermi level based on the calculation of electronic structure and ELNES. Reasons for the intens[ity] differences of the simulated and experimental spectra are discussed. This work con[tributes] to the under[standing] of ELNES and to the quantification of ELNES spectra.

1. Introduction

Electron energy loss near edge structure (ELN[ES] is [the] structure oscillation above the critical excitatio[n] energy within a 50 eV range [1]. ELNES originates from the t[ransi]tions of [core–] shell electrons to unoccupied states ab[ove] the Fermi lev[el] [2]. Generally, the unoccupied states are thought [to] consist of two parts: empty bound states and contin[uum] states. Trans[itions] to empty bound states mainly create the pe[aks] while transitions to continuum states contribute to post-peak s[pectra] which are always treated as 'background' of the ELNES. In q[uant]ification of ELNES different methods, such as simulat[ion] back[ground] with an empirical step function or using resu[lts] of tra[nsi]tions in [free] atoms, are adopted to remove the backgrou[nd] [3,4]. Unfortunately, studies of branch ratio or electron transfer betwe[en] elements based on the empirical removal method are not always su[cce]ssful. No universal solution has been reported. The main reason for [this] is that the origin of the background is still unclear. In this paper we discuss this long-standing issue and study the origin of the 'background'.

2. Materials and methods

In this study of the post-peak background we concentrate on the ELNES of atomic Ni in the forms of pure metallic Ni and NiO. For Ni atoms, there are well defined unoccupied *d* orbitals. Transitions from core–shell electrons to these orbitals generate sharp peaks in ELNES which are called 'white lines' [1]. These well defined unoccupied orbitals are localized and have relatively few effects upon other orbitals. Furthermore, experimental ELNES of pure Ni has a strong background while for NiO the background is quite weak, which gives good comparison (see Fig. 1). These properties make Ni a good subject for this study.

For pure Ni, transitions from 2*p* electrons to unoccupied states above the Fermi level are the origin of ELNES for the Ni $L_{2,3}$ edge. If transitions to continuum states create the background, then the corresponding spectrum is smooth. However, from experimental results of Ni's ELNES, there are small characteristic peaks on post-peak spectra (*e.g.* evident at 7 eV and 11 eV in Ni's spectra in Fig. 1). These peaks are difficult to explain by transitions to continuum states. On the contrary, they suggest the characteristic transitions to unoccupied orbitals. In this paper, we use *ab initio* calculation of electronic structure and spectra to show that transitions to the hybrid unoccupied orbitals can generate these features. For comparison, electronic structure and ELNES of NiO are also calculated.

Experimental ELNES data for both pure Ni and NiO are from the CEMES EELS database [5]. The electron-source voltage for the experiments was 300 kV and full width half maximum (FWHM) of the zero-loss peak was 1.1 eV. Spectrum acquisition was made in diffraction mode with a collection semi-angle of 3.5 mrad and convergence angle of 0.5 mrad [6]. With electron diffraction, single crystal grains can be selected and oriented to the [101] zone axis by tilting the sample. However, exact zone alignment is avoided in order to eliminate possible channeling which could complicate the interpretation of the inelastic scattering events [6]. In the ELNES calculation these parameters are adopted as input.

* Corresponding author. Tel.: +86 21 55274069; fax: +86 21 55270632.
E-mail address: ftian@usst.edu.cn (F. Tian).

0304-3991/$ - see front matter © 2013 Elsevier B.V. All rights reserved.
http://dx.doi.org/10.1016/j.ultramic.2013.10.008

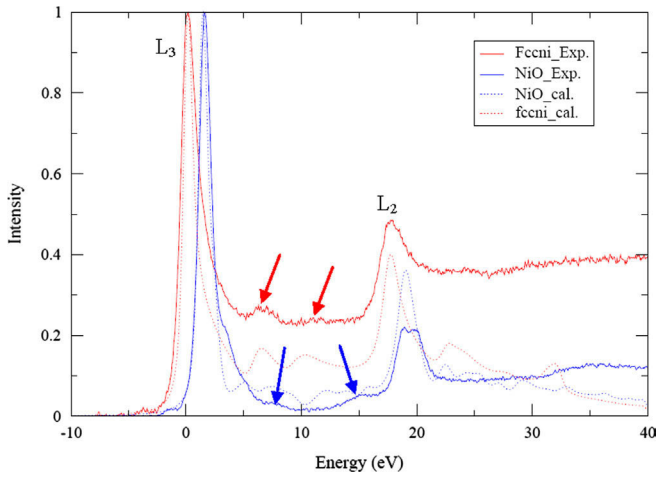

Fig. 1. ELNES of atomic Ni in pure fcc Ni (red) and NiO (blue). All spectra are normalized by setting the maxima of L_3 peaks to 1. Experimental spectra (solid lines) are aligned horizontally to the corresponding calculated ones (dotted lines) by L_3 peak positions. The red and blue arrows show the small peaks on experimental pure Ni and NiO spectra respectively. (For interpretation of the references to color in this figure caption, the reader is referred to the web version of this article.)

Table 1
Crystallographic data for the calculation of face-centered-cubic (fcc) (F) Ni and rhombohedral (R) NiO used in WIEN2K from [11]. Atomic positions of NiO are given in local coordinates of the rhombohedral unit cell to construct a supercell for antiferromagnetic calculation.

Lattice	Lattice parameters	Atom positions
F (Ni)	$a=b=c=3.5443$ Å	Ni: $x=0$, $y=0$, $z=0$
R (NiO)	$a=b=2.965169844$ Å, $c=14.526305086$ Å	Ni_1: $x=0$, $y=0$, $z=0$ Ni_2: $x=0.5$, $y=0.5$, $z=0.5$ O: $x=\pm 0.25$, $y=\pm$, $z=\pm 0.25$

The *ab initio* calculations presented in this work are performed using the WIEN2K code, which uses the linear augmented plane wave (LAPW)+local orbital method and is based on density [7]. Twenty thousand k-points are used in the Brillouin zone (BZ) integration for Ni (1470 k-points in the irreducible wedge of the BZ (IBZ)) and 100 for NiO (20 k-points in the IBZ), which are more than the reported k-points needed to achieve convergence for both self-consistent field (SCF) cycle and ELNES calculation [8]. The program generates the k-mesh in the BZ on a special point grid, which is a modified tetrahedron integration scheme [9]. In the calculation, pure Ni has a ferromagnetic fcc structure and an atomic sphere radius of 2.3 a.u. For NiO, a rhombohedral supercell contains three non-equivalent atoms as shown in Table 1 to construct an antiferromagnetic II (AFM II) type structure; in which case the radius of Ni is 2.09 a.u. and that of O is 1.85 a.u. All the parameters have been tested against numerical convergence. In the case of pure Ni a standard Perdew–Burke–Ernzerhof (PBE) type generalized gradient approximation (GGA) has been used and spin–orbit (SO) coupling is included in the calculation [10]. Whereas in the case of NiO, a modified Becke–Johnson potential (TB-mBJ)+local density approximation (LDA) correlation is included.

Originally, a BJ exchange potential is proposed to gain band gaps close to the experimental ones with a computationally cheap semi-local method within the Kohn–Sham framework. The multiplicative BJ potential is

$$v_{x,\sigma}^{BJ}(r) = v_{x,\sigma}^{BR}(r) + \frac{1}{\pi}\sqrt{\frac{5}{6}}\sqrt{\frac{t_\sigma(r)}{\rho_\sigma(r)}} \quad (1)$$

where $\rho_\sigma = \sum_{i=1}^{N_\sigma} |\psi_{i,\sigma}|^2$ is the electron density, $t_\sigma = (1/2)\ \sum_{i=1}^{N_\sigma} \nabla\psi_{i,\sigma}^{*} \cdot \nabla\psi_{i,\sigma}$ is the kinetic energy density, and

$$v_{x,\sigma}^{BR}(\vec{r}) = -\frac{1}{b_\sigma(\vec{r})}\left(1 - e^{-x_\sigma(\vec{r})} - \frac{1}{2}x_\sigma(\vec{r})e^{-x_\sigma(\vec{r})}\right) \quad (2)$$

is the Becke–Roussel potential, which is applied to describe the Coulomb potential between the exchange holes. x_σ is calculated using an equation containing ρ_σ, $\nabla\rho_\sigma$, $\nabla^2\rho_\sigma$ and t_σ, b_σ is determined by $b_\sigma = [x_\sigma^3 e^{-x_\sigma}/(8\pi\rho_\sigma)]^{1/3}$, and the asymptotic behavior of $v_{x,\sigma}^{BR}$ is that of the exact KS exchange potential [12].

The BJ potential implemented in WIEN2K is better than the LDA and PBE potentials for the description of band gaps. However, it still underestimates the band gaps significantly [13]. For further improvement, a modified BJ potential (TB-mBJ) is proposed to describe the band gaps by introducing a parameter to change the relative weights of the two terms in the BJ potential. The TB-mBJ potential is suggested as

$$v_{x,\sigma}^{TB-mBJ}(r) = c\,v_{x,\sigma}^{BR}(r) + (3c-2)\frac{1}{\pi}\sqrt{\frac{5}{12}}\sqrt{\frac{2t_\sigma(r)}{\rho_\sigma(r)}} \quad (3)$$

in which the value of the parameter c is calculated through

$$c = \alpha + \beta\left(\frac{1}{V_{cell}}\int_{cell}\frac{|\nabla\rho_\sigma(r')|}{\rho_\sigma(r')}d^3r'\right)^{1/2} \quad (4)$$

where V_{cell} is the volume of unit cell and $\alpha = -0.012$ and $\beta = 1.023$ bohr$^{1/2}$ are parameters determined by fitting to experimental values. Generally, the calculated band gap increases monotonically with respect to c, and Eq. (4) can give satisfying results to many different systems ranging from small band gap semiconductors to wide band gap insulators and transition metal oxides [14].

Compared to the LDA+U method used in the calculation of antiferromagneitc materials, the TB-mBJ potential can shift the Ni-3*d*-e_g spin down and Ni-4*s* bands in unoccupied states up simultaneously, which generates the band-gap directly according to the literature [15]. It is notable that the TB-mBJ potential is an exchange potential and not an exchange functional. Therefore, this potential should not be used for the calculation of forces, the comparison of total energies, or the optimization of the geometry [15]. Since the TB-mBJ potential does not change the shape of bands dramatically, the calculated ELNES spectra do not show dramatic change compared to those calculated by GGA+U. So the TB-mBJ potential is selected for the calculation of NiO. However, for pure Ni the exchange part of the TB-mBJ potential is much stronger than that of the LDA/PBE potentials, while the correlation function from LDA is kept constant and the good error cancellation of LDA/PBE for itinerant metallic systems has been lost [7]. So the TB-mBJ potential is not fit for the calculation of metals and GGA+SO is used for pure Ni.

In both calculations the criterion of energy convergence 0.0001 Ry and charge convergence 0.0001 e are used in the self-consistent field (SCF) calculation to obtain the fine electronic structure [16]. After SCF cycle the final Rkmax value for Ni and NiO are 6.23 and 6.93 respectively. The ELNES of pure Ni and NiO are calculated by the TELNES package in which the input parameters are selected based on experimental data as described previously. In both ELNES calculations the spectra are broadened by Gaussian broadening of 0.5 eV originating from the spectrometer. The broadening brought about by core-hole lifetime is approximately 1.4 eV and 0.55 eV for L_3 and L_2 edges respectively. Since the energy-dependent valence broadening is only accurate in a low energy range it is not used in our calculation.